Bulletin of the Seismological Society of America, Vol. 103, No. 2B, pp. 1373–1393, May 2013, doi: 10.1785/0120120157

Short-Period Source Model of the 2011 M_w 9.0 Off the Pacific Coast of Tohoku Earthquake

by Susumu Kurahashi and Kojiro Irikura

Abstract We have constructed a short-period source model for the 2011 M_w 9.0 Off the Pacific Coast of Tohoku earthquake using strong-motion records at stations near the source fault. The observed strong motions contain five wavepackets that correspond to specific strong-motion generation areas (SMGAs). The origins of the wavepackets were retrieved from the original seismograms using a semblance analysis. We determine the locations of the SMGAs based on sources extracted from the corresponding wavepackets. The short-period source model consists of five SMGAs (SMGA1–5), which are located west of the hypocenter and along the down-dip edge of the source fault. SMGA1 is located in the Miyagi-Oki source region west of the hypocenter, SMGA2 in the middle Sanriku-Oki source region north of the hypocenter, and SMGA3 in the southern Sanriku-Oki source region west of the hypocenter. SMGA4 and SMGA5 are located near the down-dip edge of the mainshock source fault, extending from offshore Fukushima prefecture to offshore Ibaraki prefecture. At some stations near the source fault, impulsive waves are also seen on the recorded seismograms. Ground motions corresponding to these impulsive waves cannot be accounted for using the conventional uniform SMGA model. We attempt instead to simulate the observed ground motions at the Onagawa Nuclear Power Plant at a depth of 128 m very near the source fault, using a heterogeneous source model. The impulsive waves are well simulated using the heterogeneous model with higher stress parameters within a small subarea inside the SMGAs.

Introduction

On 11 March 2011, an M_w 9.0 earthquake occurred off the Pacific coast of Tohoku, Japan. This was one of the largest earthquakes in terms of magnitude and consequences in the history of Japan. The huge tsunami generated by this earthquake struck the east coast along Tohoku, causing the deaths or disappearances of 19,000 people (Fire and Disaster Management Agency, 2012; see Data and Resources). The tsunami's waves were also responsible for severe accidents at the nuclear reactors at the Fukushima Daiichi Nuclear Power Plant (NPP), which exacerbated the scope of the disaster. More than 120,000 buildings were destroyed, and more than 240,000 partially collapsed.

Damage to the buildings in the region was caused mostly by the tsunami, with relatively little damage caused by tremors associated with the earthquake. In fact, one of the many unique features of the Tohoku earthquake was the relatively small amount of damage caused by ground motion. This may be due to the characteristics of the strong ground motions, which are, in turn, likely related to the rupture process for this earthquake.

Slip-distribution models for the 2011 earthquake were obtained shortly after the event using teleseismic, geodetic, and tsunami data (e.g., Fujii *et al.*, 2011; Ide *et al.*, 2011; Ozawa *et al.*, 2011; Yagi and Fukahata, 2011; Yamanaka, 2011; see Data and Resources). The Global Positioning System (GPS) and tsunami inversions reveal areas of large slip east of the earthquake's hypocenter, towards the Japan Trench. The slip distributions from broadband teleseismic *P* waves exhibit some variability and some notably dissimilar features. A unified source model was constructed by Koketsu *et al.* (2011) via the joint inversion of teleseismic, strong-motion, and geodetic datasets, using a source-fault model adopted on the basis of the distribution of aftershocks during the first 24 hours after the earthquake. Yokota *et al.* (2011) extended the unified model by incorporating a fourth dataset comprising tsunami data. Their results showed that the main rupture propagated not only in the strike direction but also in the dip direction, and extended into both the deep area called the Miyagi-Oki region and the compact shallow area near the Japan Trench.

Separate inversions of strong-motion, teleseismic, geodetic, and tsunami data tend to show frequency-dependent rupture processes. Relatively short-period generations obtained from strong-motion and teleseismic data are located

in areas down-dip of the epicenter. Most of the displacement inferred from the geodetic and tsunami data is located at depths shallower than the hypocenter, toward the trench. However, the strong-motion data used for those inversions did not include short-period motions of engineering interest in the period band from 0.1 to 10 s, as the records were band-pass filtered from 10 to 100 s.

Ishii (2011) obtained a short-period source model by applying a back-projection technique to the first *P*-wave arrival data from the Transportable Array in the U.S. with nearly 400 stations in the frequency range 0.8–2 Hz. Honda *et al.* (2011) investigated the rupture process of the Tohoku earthquake in space and time by performing a semblance-enhanced stacking analysis of the waveforms in the frequency range 0.05–0.5 Hz using the Metropolitan Seismic Observation network (MeSO-net), which spans the Tokyo metropolitan area. Their findings showed that seismic energy was generated mainly from the down-dip areas near the coasts of Miyagi and Fukushima prefectures.

Strong-motion data in the near-source region provide detailed information about the shorter-period rupture process during the Tohoku earthquake. In this study, we have determined a Tohoku earthquake source model accounting for strong ground motions by comparing the observed records from the mainshock with synthesized motions based on a characterized source model and by using the empirical Green's function (EGF) method.

Kurahashi and Irikura (2011) obtained a short-period source model consisting of five strong-motion generation areas (SMGAs) with a large slip velocity or a high stress drop. The SMGAs are distributed in the dip direction west of the Tohoku earthquake's hypocenter and in the strike direction north and south of the hypocenter, along the down-dip portion of the source fault. Similar analyses have been performed by several other research groups (Asano and Iwata, 2011; Kamae and Kawabe, 2011, see Data and Resources; Satoh, 2012). These source models are not always consistent with each other in terms of the locations and numbers of the SMGAs. Another problem with the short-period source models is that they cannot simulate impulsive waves of high acceleration and velocity in strong-motion records recorded near the source fault.

Here, we have reexamined the short-period source model, recomputing the locations, areas, and stress parameters of SMGAs. Further, a heterogeneous model is introduced for the SMGAs to simulate impulsive waves. We employed a modified approach in order to estimate strong ground motion from subduction-zone earthquakes, improving the recipe for strong-motion prediction of inland crustal earthquakes.

Strong-Motion Data

The K-NET and KiK-net strong-motion observation networks operated by Japan's National Research Institute for Earth Science and Disaster Prevention (NIED) recorded strong ground motions at more than 1000 stations during the 2011 Tohoku earthquake. Prefectures from Miyagi to Tochigi experienced very large high-frequency ground motions with peak accelerations exceeding 1000 gal at 20 stations (NIED, 2011; see Data and Resources). The strongest peak accelerations of 2933 and 2019 gal (absolute value calculated from the three components) were measured in Miyagi prefecture at K-NET stations MYG004 and MYG012, respectively, at the shortest distances of ~70–80 km from the assumed source fault.

Strong ground-motion observations near the source areas of the Tohoku earthquake were also made on the Earth's surface and underground at four NPPs: Onagawa, Fukushima–Daiichi, Fukushima–Daini, and Tokai–Daini. The maximum acceleration on the rock surface at the Onagawa NPP was 567.5 gal, ~123 km away from the epicenter. Other organizations such as the Port and Airport Research, Building Research, and Public Works institutes have also recorded strong ground motions near the source areas.

In this study, we have applied semblance analysis to several wavepackets observed on strong-motion seismograms in small arrays formed by three to four stations of the strong-motion network in order to determine the location of the SMGAs. We have used strong-motion data from a total of 21 KiK-net, K-NET, and Onagawa NPP stations for the analysis.

We have also used strong-motion data recorded at 14 underground KiK-net stations in the near-source regions between Iwate and Ibaraki prefectures and at one of the underground stations of the Onagawa NPP, to further constrain the short-period source model. The observed records used as EGFs were band-pass filtered from 0.15 to 10 Hz, based on the reliable frequency range observed for small events.

Locating Strong-Motion Generation Areas

The strong-motion stations that recorded the 2011 Tohoku earthquake are shown in Figure 1a. The acceleration records at stations along a north–south line are displayed with identical time and amplitude scales (Fig. 1b). We recognize five isolated wavepackets (WP1, WP2, WP3, WP4, and WP5) in the aligned records, arriving from different positions on the source fault. We consider those positions to correspond to the SMGAs.

The source fault plane is defined to be 450 km long and 200 km wide with a strike of 193° and a dip of 10°, based on the distribution of the first 24 hours of aftershocks and the Centroid Moment Tensor solution issued by the Japan Meteorological Agency (JMA) as shown in Figure 2. The hypocenter (marked by a star in Fig. 2) was at 38.103° N, 142.861° E, and was 23.7 km deep according to the JMA.

We first assume that the SMGAs are located on the source fault plane. Kurahashi and Irikura (2011) determined the locations of the SMGAs and the optimum *S*-wave and rupture velocities between the mainshock hypocenter and the SMGAs, by picking the onset times of wavepackets visible on the strong-motion seismograms from the underground KiK-net

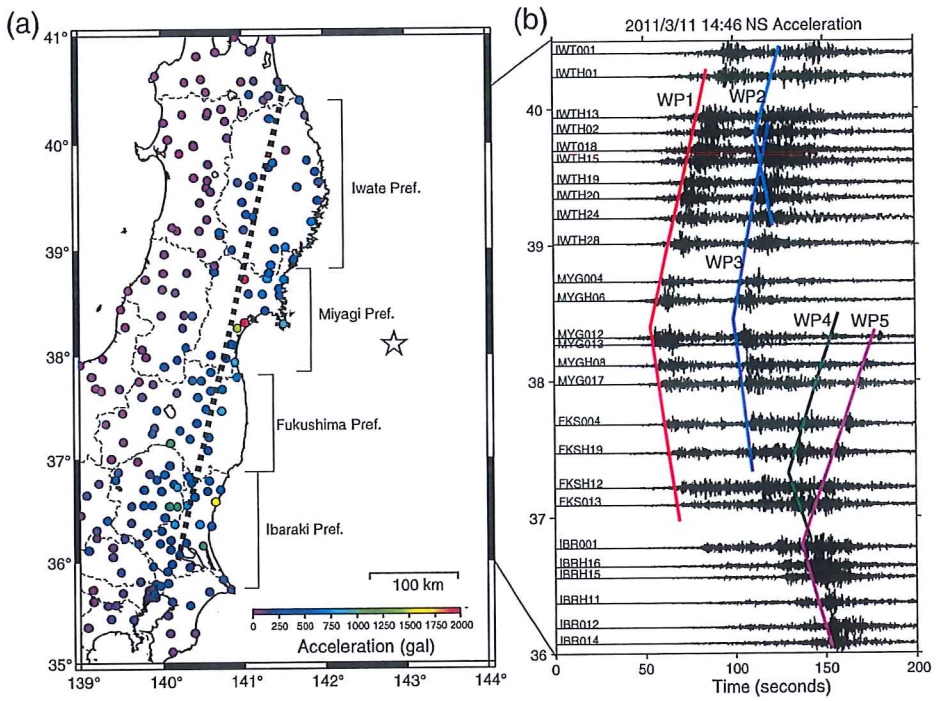

Figure 1. (a) Map showing the location of observation stations. (b) Acceleration seismograms at stations plotted in order from north to south. The colored lines indicate the travel times of *S* waves generated from five strong-motion generation areas (SMGAs). Red, sky-blue, blue, green, and pink represent *S* waves propagating from SMGA1, SMGA2, SMGA3, SMGA4, and SMGA5 to the stations, respectively.

sites. Their results showed that WP1, WP2, WP3, WP4, and WP5 arrived from SMGA1, SMGA2, SMGA3, SMGA4, and SMGA5, respectively, located near the down-dip edge of the mainshock-source fault, extending from offshore Miyagi Prefecture to offshore Ibaraki prefecture (Fig. 2).

However, the locations of the SMGAs were not well constrained by the onset times used in the research of Kurahashi and Irikura (2011). The precision of the SMGAs' locations is controlled by the uncertainty in picking onset times, which have a range of uncertainties as the onsets of the wavepackets are not always impulsive. It is highly difficult to identify direct *S* waves at many stations from an identical source using onset times only, particularly when the number of available stations is limited.

In this study, we have therefore reestimated the locations of the SMGAs using a semblance analysis of the wavepackets seen on strong-motion seismograms in order to more accurately determine short-period source models. The wavepackets WP1, WP3, and WP5 are easily extracted from the observed seismograms because they form isolated wavelets (Fig. 1b). A similar analysis was made by Honda *et al.* (2008) to determine the location of an asperity that ruptured during the 2003 Tokachi-Oki earthquake using the K-NET and KiK-net strong-motion networks and the high-sensitivity seismograph network (Hi-net).

We have grouped the strong-motion stations near the source fault into seven arrays, A–G, each of which consists of three or four neighboring stations (Fig. 3). For each of these arrays, we undertake semblance analysis of the wavepackets to estimate their arrival azimuths. Before starting the semblance analysis, we have verified that the wavepackets at each array consisted of predominantly *S* waves arriving from identical sources. If this were not the case, noise would not be cancelled out by the semblance analysis, resulting in spurious features, or ghost waves, as the numbers of stations in each array is very small.

As an example of the analysis, Figure 4 illustrates the observed acceleration seismograms and particle motion diagrams of *P* and *S* waves in the horizontal and vertical planes, recorded at a depth of 128 m at the Onagawa NPP. The horizontal orbits of the *P* waves of WP1 indicate that the waves arrive from an approximately southeast direction (Fig. 4a), whereas those of the *S*-waves are polarized perpendicular to the *P* waves. The *S*-wave radial- and vertical-particle motion diagrams in the vertical plane are clearly perpendicular to the orbits of the *P* waves in Figure 4b, consistent with a typical *SV*-wave feature.

The particle motion diagrams in the horizontal and vertical planes for the *P*- and *S*-wave portions of WP3 (Fig. 5) have almost the same features as those shown in Figure 4, confirming that the waveforms of WP3 are predominantly *S* waves.

Figure 6 shows radial-component waveforms and vertical-plane, particle motion diagrams of WP1 at three stations in array B. The corresponding figures for WP3 at three stations in array C are shown in Figure 7. We infer from these

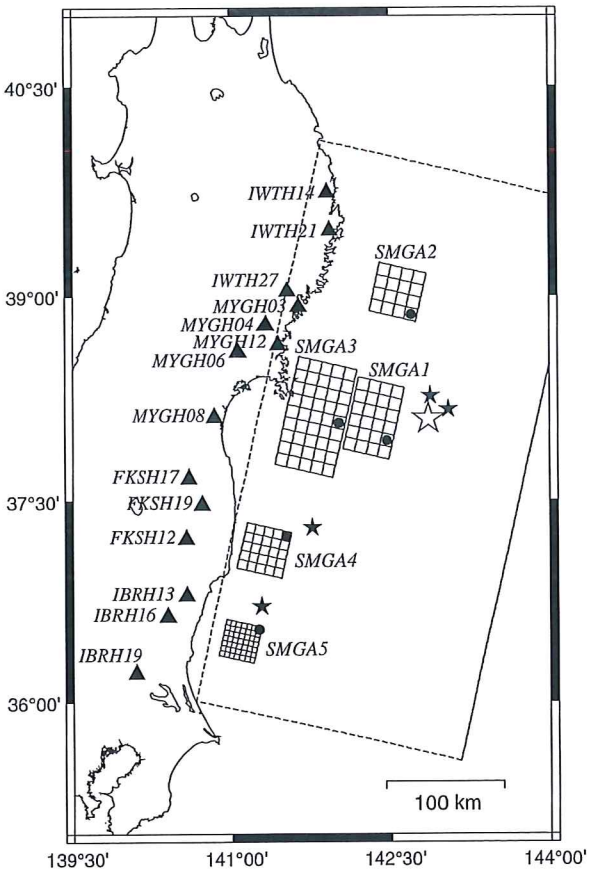

Figure 2. Characterized source model for the 2011 M_w 9.0 Off the Pacific Coast of Tohoku earthquake obtained by Kurahashi and Irikura (2011). The open star shows the epicenter of the mainshock. The closed stars show the epicenters of the events used as the empirical Green's functions (EGFs). The small rectangles and closed circles inside them show the strong-motion generation areas (SMGAs) and their initiation points. The closed triangles mark KiK-net stations used for the analysis.

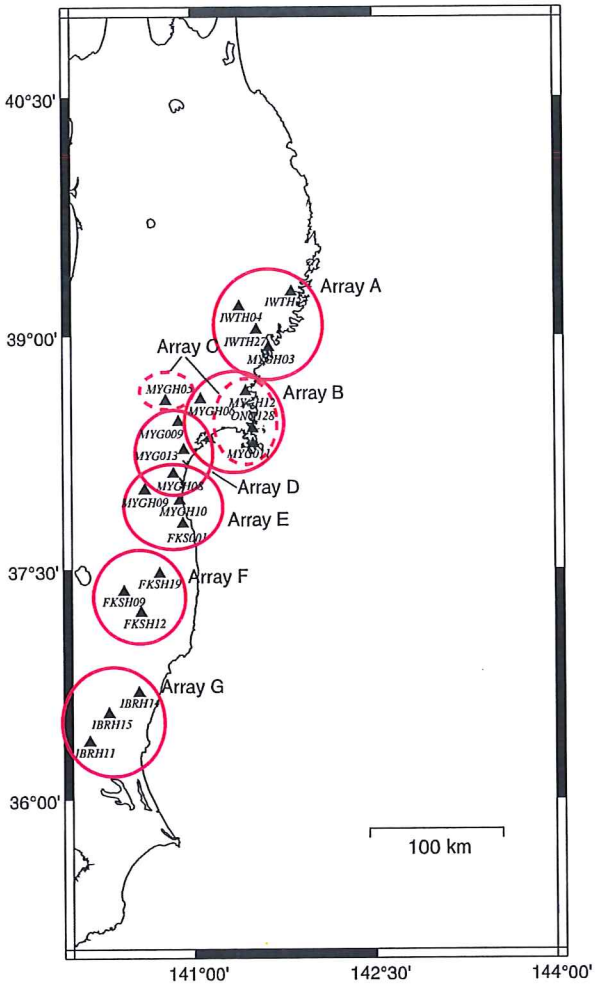

Figure 3. Map showing arrays A–G used in the semblance analysis. The closed triangles indicate KiK-net and K-NET stations.

results that the waveforms identified as WP1, WP3, and WP5 in the arrays consist predominantly of *S* waves. Based on these findings, waveforms with durations of 3 s and exhibiting *SV*-wave orbits were used for our semblance analysis.

We next attempt to estimate the locations of the SMGAs as the presumed origins of wavepackets WP1, WP3, and WP5. The propagating azimuth and apparent velocities of the wavepackets in each array were estimated by semblance analysis. The semblance value, S, for a particular time window is calculated by

$$S(s) = \frac{\sum_{k=1}^{M}\left[\sum_{i=1}^{N} u(x_i, t_k + sx_i)\right]^2}{\sum_{k=1}^{M}\sum_{i=1}^{N} u(x_i, t_k)^2},$$

where N is the number of stations in an array, and M is the number of time samples in a time window. The term $u(x_i, t_k)$ is the waveform observed at the ith site at time t_k. The term x_i is defined as the distance $(x_i'–x_r)$, where x_r is the distance between the reference site and an assumed origin, and x_i' is the distance between the origin and the ith site. V_S is the S-wave velocity. The term s is the slowness, which is the inverse of the S-wave velocity. In order to reduce the noise introduced by the arrangement of stations, we average the initial semblance values obtained for the two horizontal components. Hereafter, we refer to the averaged semblance values as the semblance value.

We locate the source areas assumed to correspond to WP1, WP3, and WP5 using the same approach as that employed by Honda *et al.* (2008). This method was originally developed by Spudich and Oppenheimer (1986). The semblance values are projected onto an assumed source area on the mainshock fault plane using seismic ray tracing in a uniform velocity model. We calculate the semblance values taking into account the travel time from the assumed source

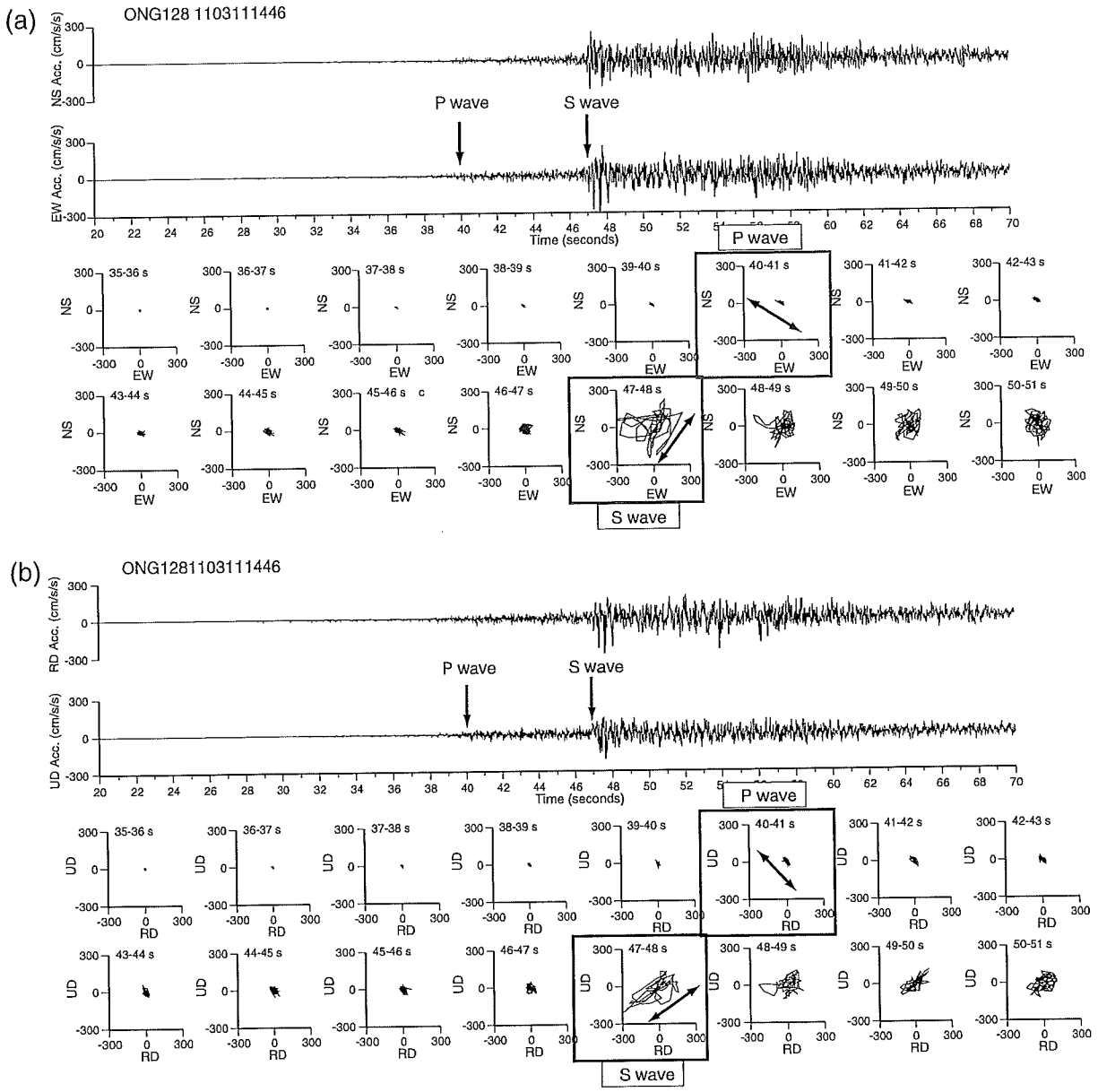

Figure 4. Observed acceleration waveforms at ONG128 (Onagawa Nuclear Power Plant [NPP]) at a depth of 128 m and particle motion diagrams for a time window of 1 s. The arrows indicate the onsets of the *P* and *S* waves of wavepacket 1 (WP1). (a) Horizontal plane motions (north–south and east–west components). (b) Vertical plane motions (radial and UD components).

areas to the stations in each array. The analysis required for a given wavepacket can be performed independently of that for the other wavepackets, as the seismograms are temporally distinct from each other.

The assumed source area corresponding to the origin of each wavepacket is located on the fault plane, as shown in Figure 8. The location and area are refined after preliminary analysis, namely an approximate estimation of the origin time from the onset times of the wavepackets at multiple stations. The assumed areas for WP1, WP3, and WP5 are set to be 110×110 km^2, divided into 11×11 elements.

The velocity waveforms of the three wavepackets were extracted in 3-s-wide windows after band-pass filtering between 0.1 and 10 Hz. First, the travel times sx_r between the reference site and the assumed origin, and sx_i' between the ith site and the assumed origin in each array were calculated assuming an average *S*-wave velocity, and then the travel time differences sx_i between the reference site and

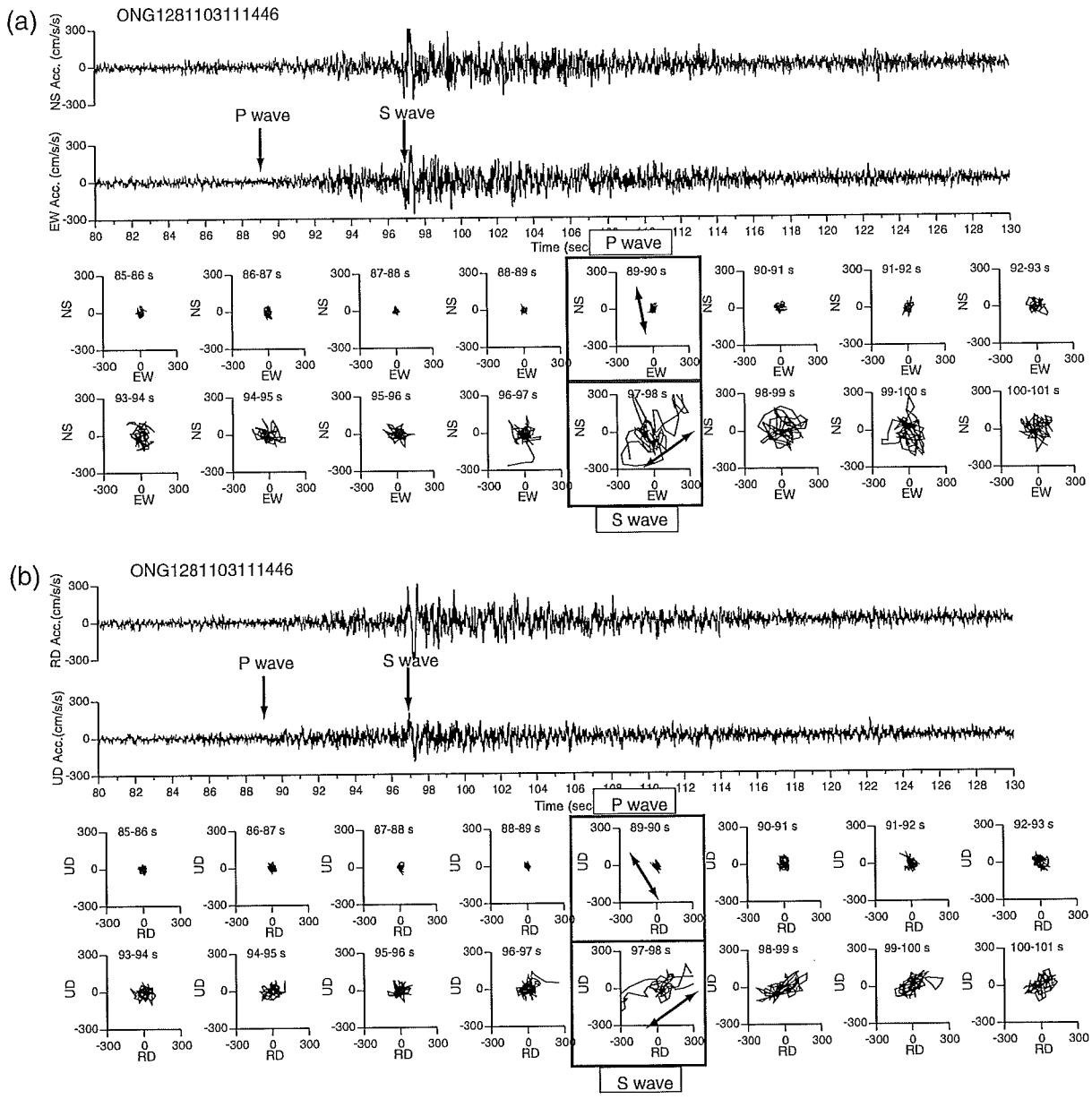

Figure 5. Observed acceleration waveforms at ONG128 (Onagawa Nuclear Power Plant [NPP]) at a depth of 128 m, and particle motion diagrams for a time window of 1 s. The arrows indicate the onsets of the *P* and *S* waves of wavepacket 3 (WP3). (a) Horizontal plane motions (north–south and east–west components). (b) Vertical plane motions (radial and UD components).

the *i*th site were calculated to be $sx_i = sx'_i - sx_r$. The slowness is assumed to lie in the range of 1/2.0–1/4.0 s/km.

We have confirmed that the semblance values are maximized for an *S*-wave velocity of 3.8 km/s. Figure 8 shows the semblance value distributions using arrays A, B, and E for WP1; arrays C, D, and E for WP3; and arrays F and G for WP5.

Assuming a certain distance between the origin of each wavepacket and the array centroid (illustrated as a circle in each panel of Fig. 8) and an *S*-wave velocity of 3.8 km/s, we can calculate the semblance values as a function of incident azimuth (Fig. 9). The azimuths with the maximum semblance values correspond to the propagation direction from the origin of the wavepacket to the arrays. As expected, each array shows a different azimuth from the origin to the array centroid. These propagation azimuths for the arrays intersect at points inferred to mark the origins of the wavepacket—specifically, the locations of the SMGAs (Fig. 10).

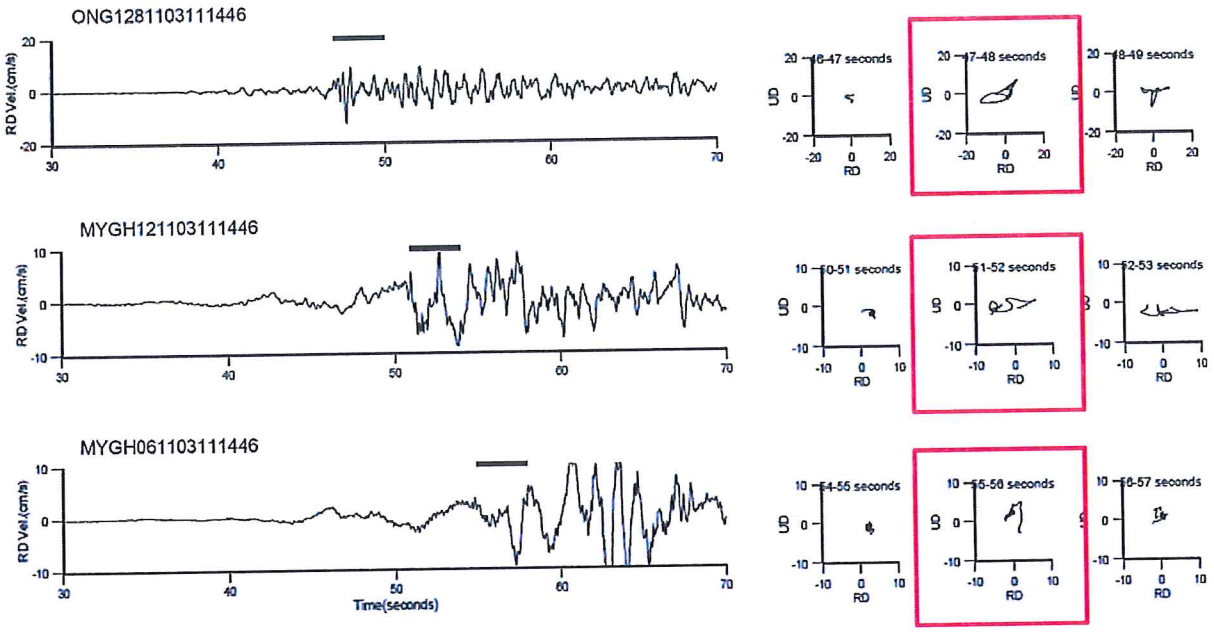

Figure 6. Observed velocity waveforms of the radial component at ONG128 (Onagawa Nuclear Power Plant [NPP]), MYGH12 (KiK-net Sizugawa), and MYGH06, and vertical particle motion diagrams showing the radial and UD components for a time window of 1 s surrounding the onset time of wavepacket 1 (WP1).

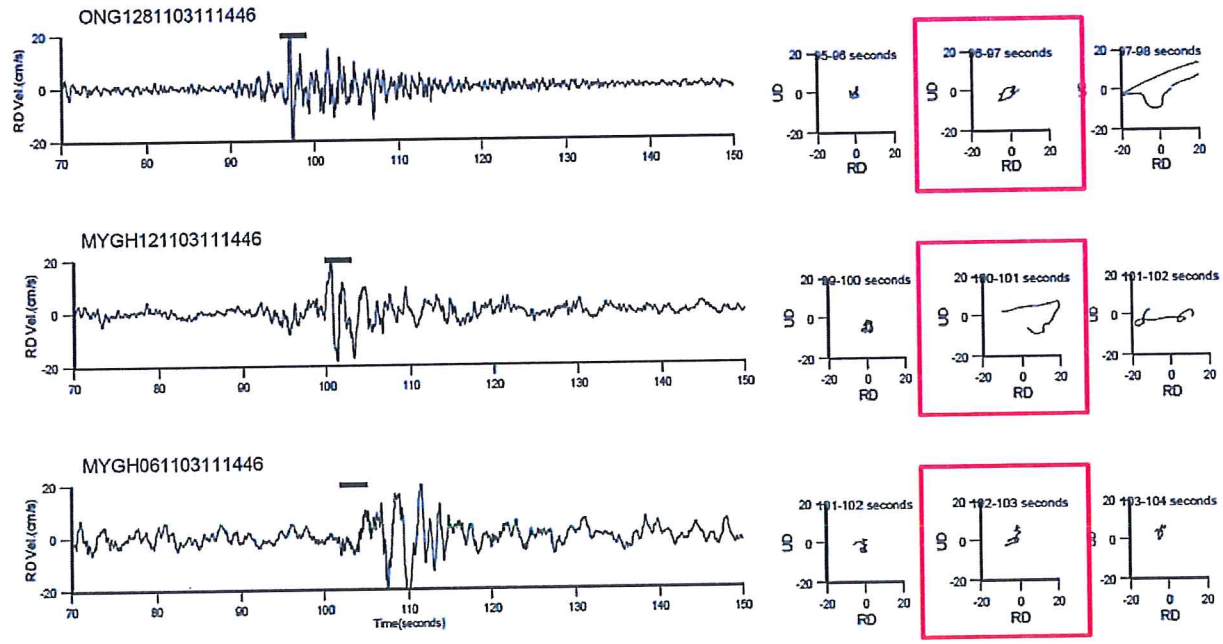

Figure 7. Observed velocity waveforms of the radial component at ONG128 (Onagawa Nuclear Power Plant [NPP]), MYGH12 (KiK-net Sizugawa), and MYGH05, and vertical particle motion diagrams showing the radial and UD components for a time window of 1 s surrounding the onset time of wavepacket 3 (WP3).

The results of our semblance analysis show that the locations of SMGA1 and SMGA5 corresponding to WP1 and WP5 are almost the same as those identified by Kurahashi and Irikura (2011) using the back-propagation method (Kurahashi and Irikura, 2010), whereas the location of SMGA3 is different, situated to the east of SMGA1. The

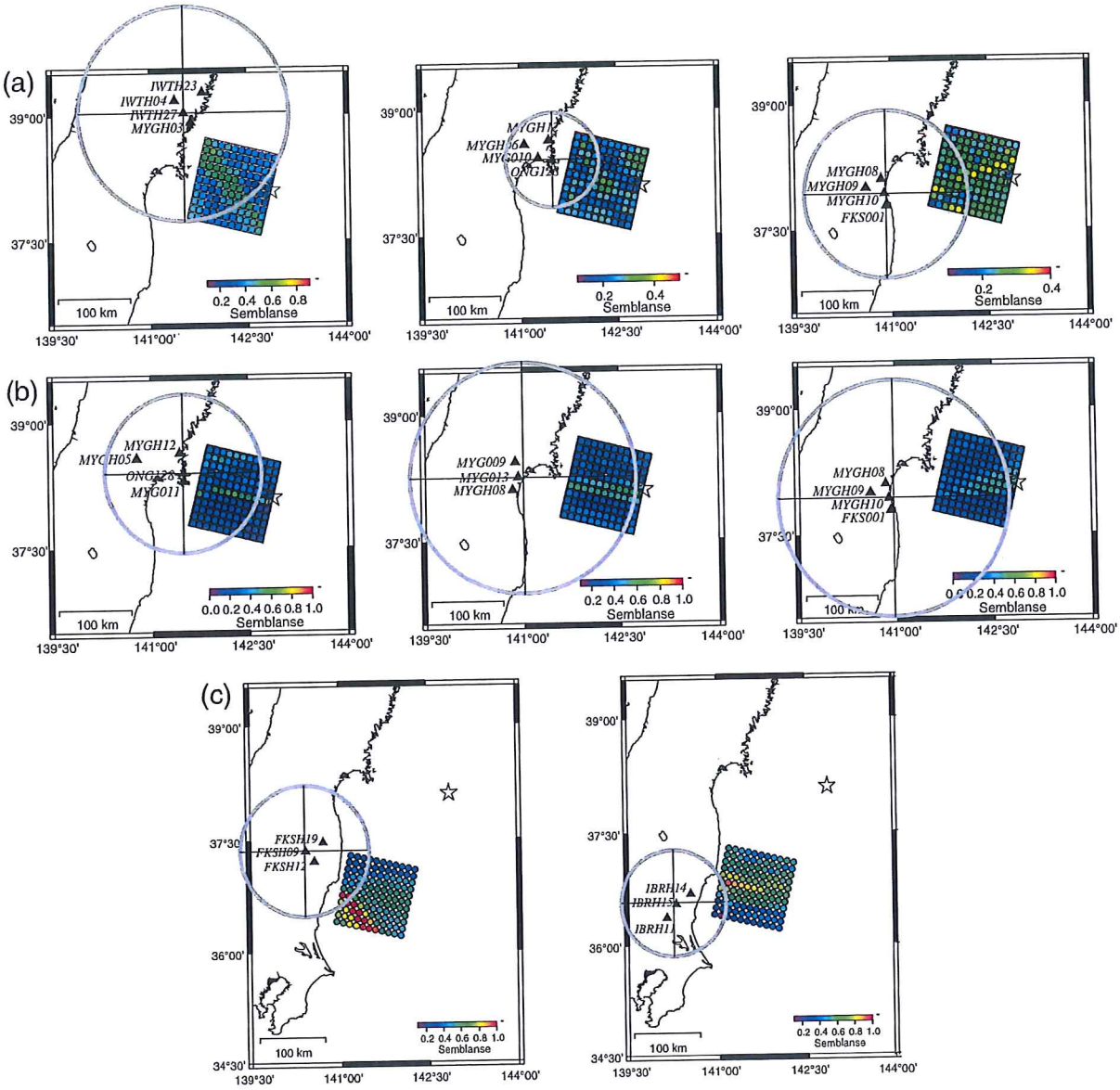

Figure 8. Semblance value distribution obtained for arrays A–G. (a) The top three panels show the semblance values on the assumed source for wavepacket 1 (WP1), the middle three panels show those for wavepacket 3 (WP3), and the bottom two panels show those for wavepacket 5 (WP5).

reason why the location of SMGA3 differs from that obtained previously is likely to be that we have used much more data, including high-quality, strong-motion seismograms such as those recorded at MYGH12 (KiK-net Sizugawa) at a depth of 105 m very near the mainshock source fault and those at ONG128 (Onagawa Nuclear Power Plant) at a depth of 128 m. On this basis, and because the SMGA locations have been obtained using two methods, semblance analysis, and back propagation, the SMGA locations obtained in this study are thus inferred to be more reliable than those of the previous study (Kurahashi and Irikura 2011).

Short-Period Source Model and Ground-Motion Simulation

Strong-motion data from the near-source region provide detailed information about the short-period rupture process during an earthquake (e.g., Kamae and Irikura, 1998; Kurahashi *et al.*, 2008). In the second phase of this study, we have estimated a short-period source model consistent with observed strong ground motions produced by the Tohoku earthquake using a characterized source model and the EGF method. The observed strong ground motions from this

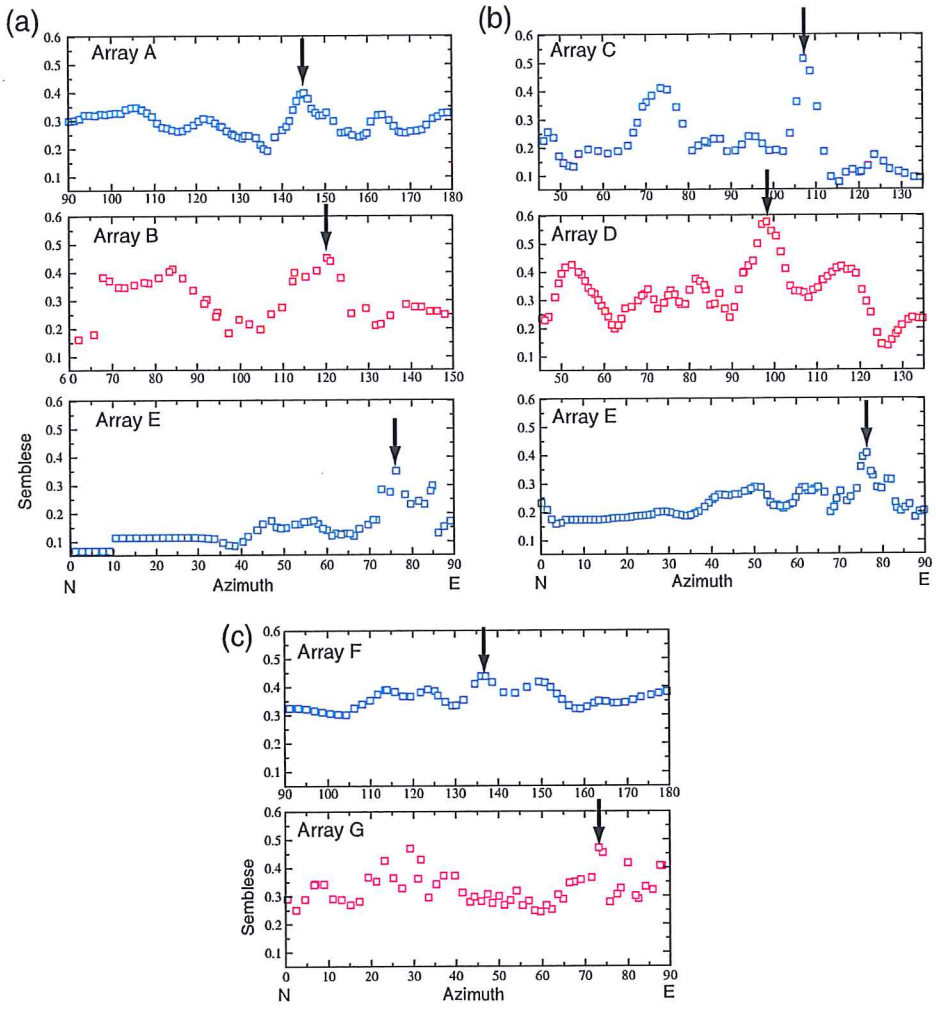

Figure 9. Semblance values as a function of propagation azimuth for wavepacket 1 (WP1), wavepacket 3 (WP3), and wavepacket 5 (WP5) in arrays A–G. The average *S*-wave velocity is fixed as 3.8 km/s. Arrows indicate the optimum propagation azimuths of WP1, WP3, and WP5 in each array.

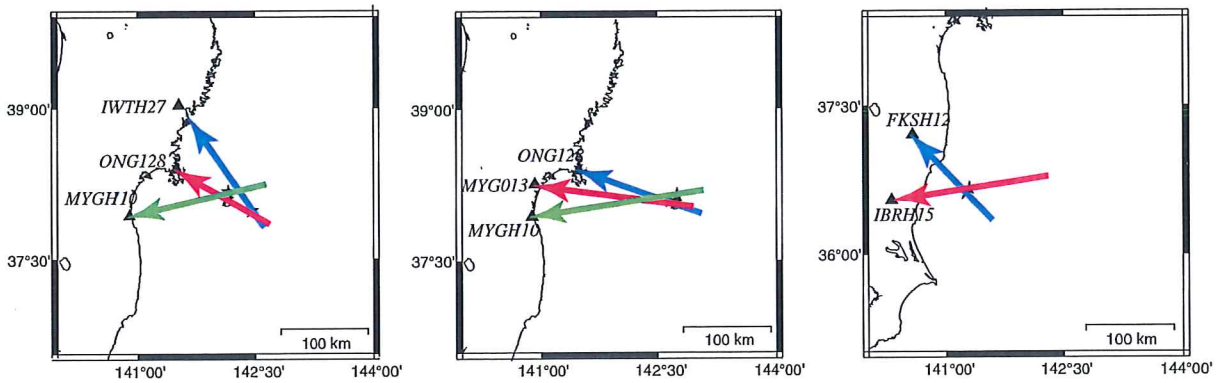

Figure 10. Origins of wavepacket 1 (WP1), wavepacket 3 (WP3), and wavepacket 5 (WP5) determined from the propagation azimuths optimized by the semblance analysis illustrated in Figure 9.

earthquake consisted of five isolated wavepackets originating from the five SMGAs previously described.

Empirical Green's Function for Simulation of Strong Ground Motion

The sizes of events used as the EGFs should ideally be much smaller than the size of each SMGA. Moreover, the records of EGF events used must share common propagation paths, site effects, and radiation characteristics with the ground motions from SMGAs of interest.

To calculate ground motions for each SMGA, we divide the area of the SMGA into N × N square subfaults, the uniform area of which is set to be the same as the area of the event used as the EGF. The ground motions from the SMGAs are expressed as a superposition of the EGFs. Irikura and Kamae (1994) indicated that the simulated spectra using the EGF method exhibit depleted amplitudes in the intermediate frequency range when the number of superimposed EGFs increases. Consequently, care must be taken to choose EGF events of suitable size. In the present study, events with $M > 6.0$ were required to satisfy the condition described by Irikura and Kamae (1994).

As noted above, another important requirement is that EGF events are selected that have similar propagation paths to the SMGAs in question. The 2005 M_w 7.2 Miyagi-Oki earthquake occurred close to both SMGA1 and SMGA3. We therefore use recordings of this event, referred as event A in Table 1, as EGFs for SMGA1 and SMGA3. Furthermore, event A is also adopted as an EGF for SMGA2 because there are no appropriate events near SMGA2.

The EGFs for SMGA4 and 5 are referred to below as event B (M_w 6.0) and event C (M_w 5.7), respectively. The source parameters of events A, B, and C are listed in Table 1. We did not estimate the waveforms of WP4 and WP5 at ONG128, as the strong-motion records of events B and C are unavailable.

Seismograms produced by the 2005 Miyagi-Oki earthquake, event A, at ONG128 and MYGH04 are shown in Figure 11. Event A itself is inferred to have involved two SMGAs, because the *S*-wave portions of the seismograms consist mainly of two wavepackets (Suzuki and Iwata, 2007). For the purposes of this study, we use the second of these two wavepackets as the EGF. The second wavepacket contains not only the ballistic *S*-wave signal but also the *S*-wave coda, whereas the first wavepacket contains no coda information as

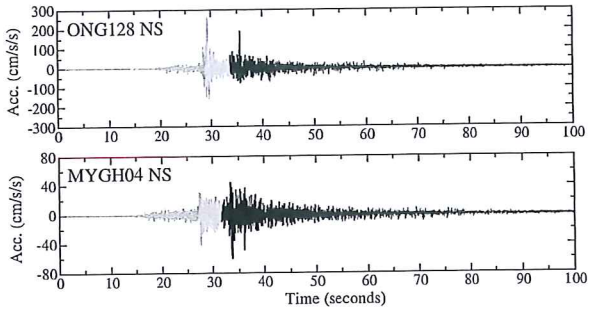

Figure 11. Observed seismograms at ONG128 (Onagawa Nuclear Power Plant [NPP]) and MYGH04 from the 2005 Miyagi-Oki earthquake (event A). Waveforms for the second wavepacket are used as empirical Green's functions (EGFs) at the observation stations.

it is truncated by the second. Conversely, the second wavepacket could be affected by the *S*-wave coda parts from the first wavepacket. To investigate these possible effects, we have compared the synthetic motions of the two wavepackets. The synthetic waveforms are almost the same in terms of peak amplitude and envelope, indicating that the influence of the coda of the first wavepacket on that of the second is small.

We estimate the displacement source spectra of events A–C using underground records from KiK-net stations where the *S* wave exceeds 2000 m/s (Fig. 12), and where site effects can thus be inferred to be minimal. The source spectra are obtained by removing propagation-path effects from the observed spectra. We use the Q values described by Kawase and Matsuo (2004) to estimate propagation-path effects, and adopt the seismic moment of event A reported by Suzuki and Iwata (2007) and that of event B from the NIED seismic-moment tensor catalog. The corner frequencies of these spectra were determined by fitting omega-squared models. The source areas and stress parameters are estimated from the seismic moments and corner frequencies using Brune's (1970, 1971) formula. We use an *S*-wave velocity of 3.8 km/s. The source parameters of the EGF events are listed in Table 2.

Forward Modeling of the Short-Period Source Model

We have simulated the ground motions for the characterized source model using the EGF method (Irikura, 1986)

Table 1
Source Parameters of Events A–C Used as Empirical Green's Functions

Name	Event A	Event B	Event C
Origin time (JST)	2005/08/16 11:46	2007/11/26 22:51	2009/02/01 6:52
M_w	7.2	6.0	5.7
dl, dw (km)	8.5, 8.5	7.7, 7.7	4.4, 4.4
Stress parameter (MPa)	20	4.2	10.4
M_0 (N·m)	5.23×10^{18}*	7.66×10^{17}	4.65×10^{17}

*Only for strong-motion generation area 2 (SMGA2) Suzuki and Iwata (2007).

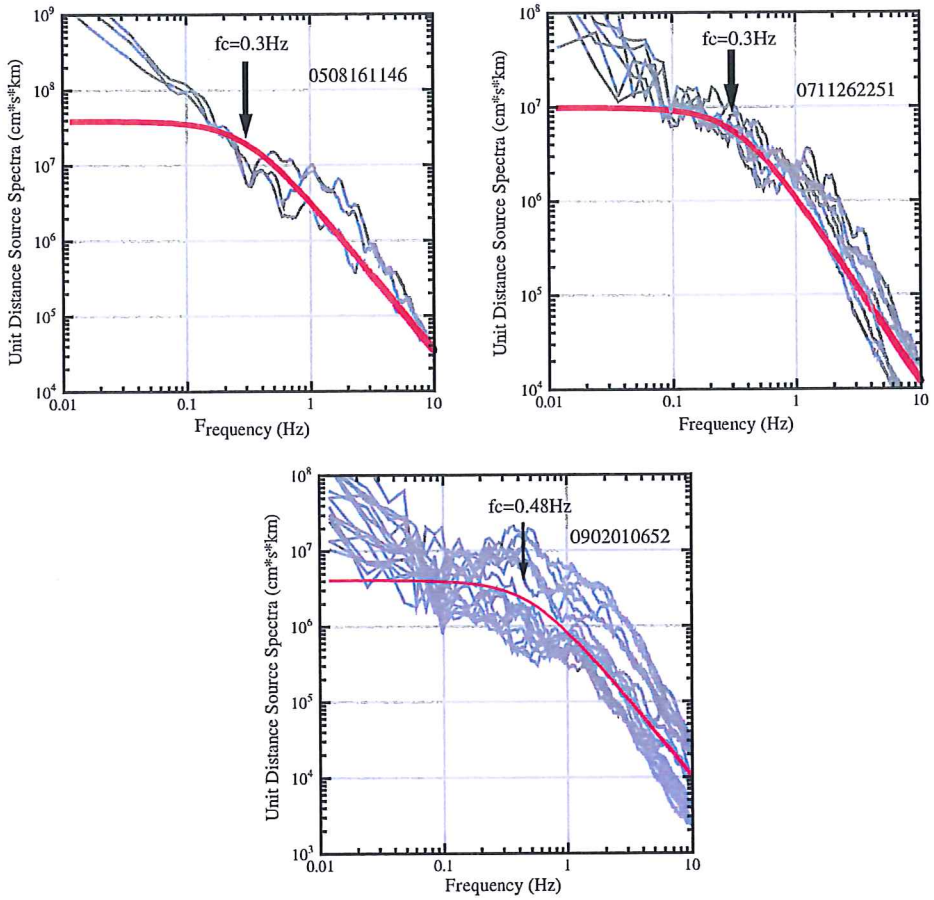

Figure 12. Empirical Green's function (EGF) displacement source spectra at underground stations in rock for events A–C.

and a revised method (Irikura *et al.*, 1997). We omit details of the EGF method here as they have been explained in previous research (e.g., Kamae and Irikura, 1998; Kurahashi and Irikura, 2010). The rise time inside each SMGA is given as $W_s/4V_r$ (where W_s is the width of the SMGA and V_r, the rupture velocity), following empirical relations presented by Kataoka *et al.* (2003). The average *S*-wave velocity is given as 3.8 km/s based on Ts-p times versus arrival times at observed stations. The total ground motions at each station are calculated by summing the contributions from all of the SMGAs, offset according to the delay times for the SMGAs with respect to the mainshock origin time, and the arrival times from the initiation points of the SMGAs to the station.

The process of determining the locations of the five SMGAs involves the following criteria:

1. The locations of SMGAs 1, 3, and 5 are determined based on the semblance analysis.
2. SMGA2 and SMGA4 are estimated by the back-propagation method (Kurahashi and Irikura, 2010) because the waveforms of WP2 and WP4 are not isolated on the observed seismograms.

Table 2
Source Parameters of the Strong-Motion Generation Areas (SMGAs) Identified in This Study

	L (km)	W (km)	M_0 (N·m)	Stress Parameter (MPa)	Rupture Delay Time from Origin Time (s)
SMGA1	34.0	34.0	2.68×10^{20}	16.0	24.5
SMGA2	25.5	25.5	1.41×10^{20}	20.0	66.5
SMGA3	42.5	42.5	6.54×10^{20}	20.0	66.5
SMGA4	23.1	23.1	1.24×10^{20}	25.2	117.5
SMGA5	35.2	35.2	5.95×10^{20}	26.0	127.5

The optimum source model is selected so as to minimize the residuals between the observed and synthetic ground motions, defined by the following equation (Miyake *et al.*, 1999):

$$\text{Residual values} = \sum_{\text{station}} \sum_{\text{Component}} \left\{ \sum_t (u_{\text{obs}} - u_{\text{syn}})^2 \Big/ \left[\left(\sum_t u_{\text{obs}}^2 \right) \left(\sum_t u_{\text{syn}}^2 \right) \right]^{1/2} + \sum_t (a_{\text{env,obs}} - a_{\text{env,syn}})^2 \Big/ \left(\sum_t a_{\text{env,obs}} \right) \times \left(\sum_t a_{\text{env,syn}} \right) \right\}.$$

The first and second terms represent the sum of the squared residuals of displacement seismograms and acceleration envelopes, respectively. The parameters which characterize each SMGA are its rupture starting point, location, and stress parameters.

The best-fitting short-period source model consisting of five SMGAs is obtained by minimizing the fitting function described in the previous section. The area and initiation point of each SMGA and the epicenters of events A, B, and C are shown in Figure 13. The source parameters of the final source model, particularly the length, width, seismic moment, stress parameter, and rupture delay time for each SMGA with respect to the origin time are listed in Table 2.

Figure 14 illustrates comparisons between the observed and synthetic waveforms in the form of acceleration, velocity, and displacement. The synthetic waveforms at most of stations fit the observations reasonably well, but impulsive waves observed at some stations near the source fault are not reproduced by the synthetic waveforms.

Figure 15 shows a comparison of the locations of SMGAs obtained in the present study with those identified by Asano and Iwata (2011; see Data and Resources) and Satoh (2012). Our new estimates of the sources of WP1 and WP3 coincide well with the previous results, although the areas of SMGA1 and SMGA3 are not entirely consistent.

Heterogeneity inside the SMGAs

The global features of the short-period ground motions, acceleration, and velocity seismograms can largely be accounted for using the five SMGAs with a uniform-stress parameter, as previously described. In detail, however, impulsive waves observed at some stations near the source fault are not consistently simulated using the simple source model. For example, the observed ground motions at ONG128, one of the stations closest to the source fault, exhibit remarkably impulsive waves in the initial portions of WP1 and WP3, and these features cannot be explained by the simulations described at this time.

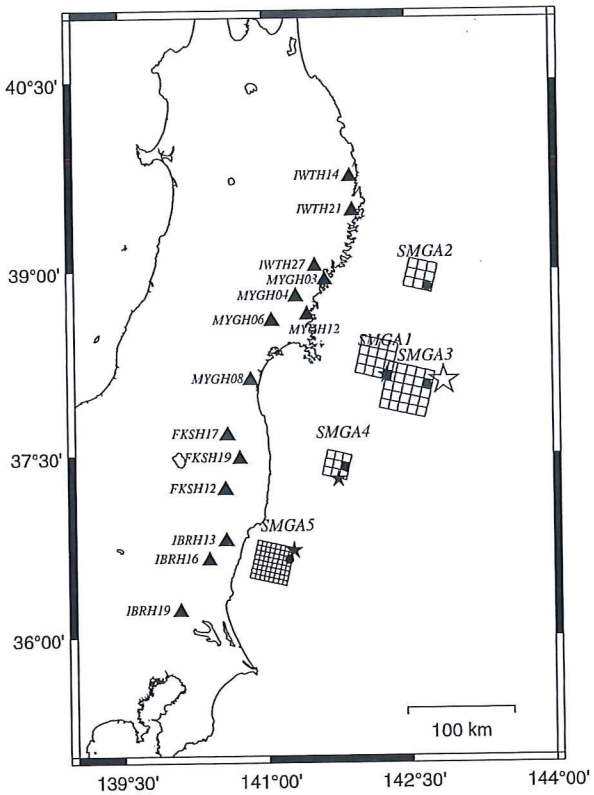

Figure 13. Short-period source model consisting of five strong-motion generation areas (SMGAs; meshed rectangles). The large open star denotes the mainshock epicenter; closed stars, the epicenters of EGF events; and closed circles, the initiation point of each SMGA.

Impulsive waves are also observed at other stations, propagating from near-source to far-source stations as shown in Figure 16. Similar ground motions containing impulsive waves were reported at Kaihoku Bridge during the 1978 M_w 7.4 Miyagi-ken-Oki earthquake by Matsushima and Kawase (2006) and at TKCH07 (Toyokoro) during the 2003 Tokachi-Oki earthquake by Nozu and Sugano (2006) and Nozu *et al.* (2009). Those authors showed that such impulsive ground motions could be explained by modeling a small subarea with higher stress parameters inside an asperity, which is called a super asperity.

We have attempted to simulate the observed ground motions at ONG128 more accurately by assuming that the SMGAs related to WP1 and WP3 have heterogeneous stress parameters. That is, each SMGA has a small subarea with higher stress parameters inside the area with uniform stress parameters, as shown in Figure 17. A comparison between observed and synthetic acceleration and velocity seismograms at ONG128 using the heterogeneous model is presented in Figure 18. The impulsive waves of WP1 are well simulated using a heterogeneous model containing a subarea whose stress parameters are a factor of two higher than those in the surrounding area. However, those of WP3 are

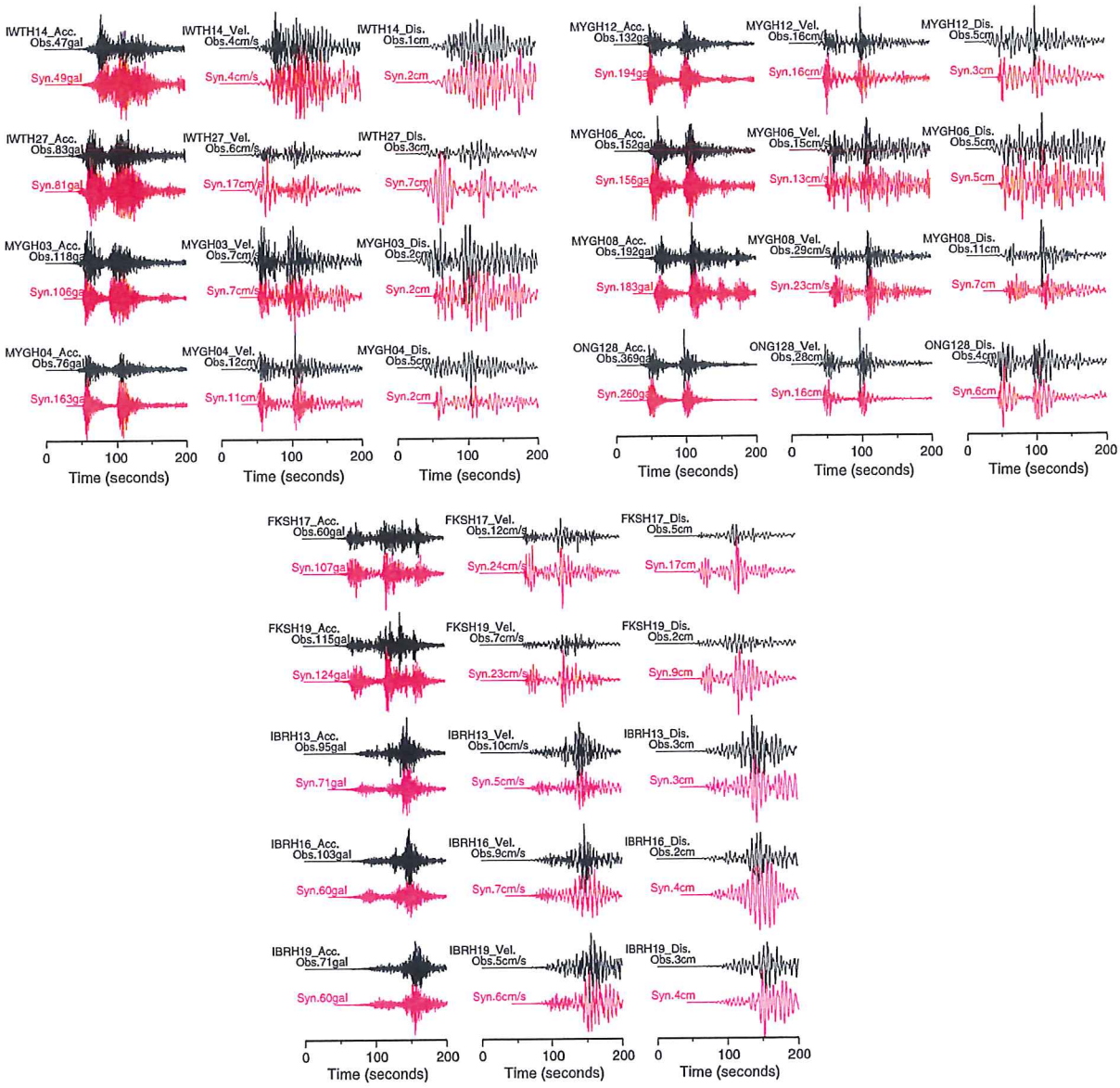

Figure 14. Comparison of the observed and synthetic seismograms (north–south component) obtained using the empirical Green's function (EGF) method at underground KiK-net and Onagawa Nuclear Power Plant (NPP) stations.

well simulated when the subarea's stress parameters are higher by a factor of four. The other three wavepackets exhibit no distinct impulsive waves.

The scale of heterogeneity inferred in this analysis is affected by the size of the EGF event employed. To investigate the size of the heterogeneity in more detail, records from smaller events should be used as the EGF.

A similar analysis of impulsive waves from the 2011 Tohoku earthquake was conducted by Nozu (2012). He showed that the strong ground motions from the 2011 Tohoku earthquake were well simulated using nine super asperities. His simulations were made using EGFs of $\sim M_w$ 6. The sizes of the super asperities inferred in that study are almost the same as those of the high-stress sub-areas identified here.

The five SMGAs in this study are superimposed on the nine super asperities identified by Nozu (2012) in Figure 19. Two of the nine super asperities, SA1_1 and SA2, coincide with the subareas of higher stress parameters inside SMGA1 and SMGA3, respectively. In Nozu's analysis, SA2 has the highest short-period levels of the nine super-asperities and SA1_1 has the second highest. Qualitatively, our results concerning heterogeneous SMGAs agree well with those of Nozu (2012).

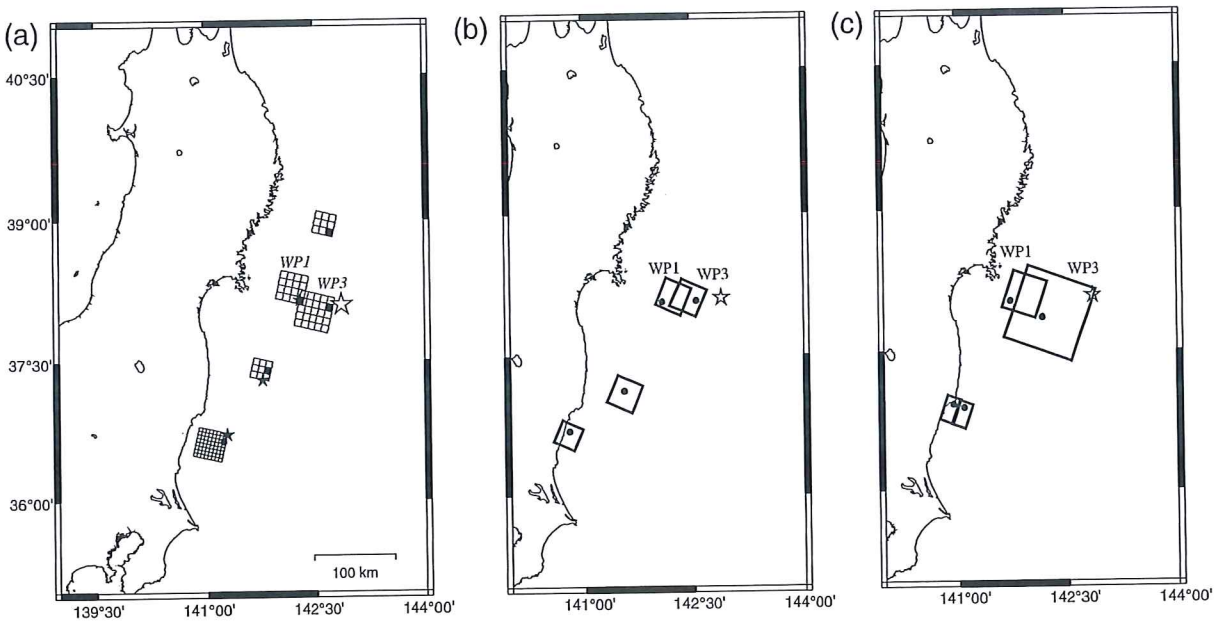

Figure 15. Comparison of the short-period source models obtained in this present study with those of Asano and Iwata (2011; see Data and Resources) and Satoh (2012).

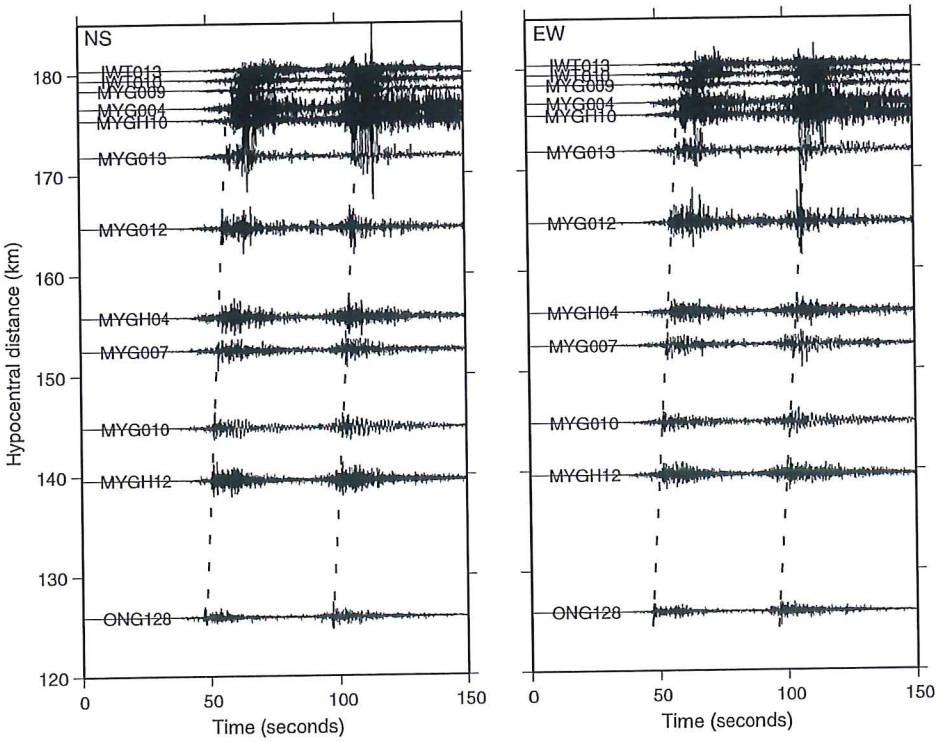

Figure 16. Observed acceleration seismograms at strong-motion stations in Miyagi prefecture near the source fault of the mainshock. Data from a few stations in Iwate prefecture are also included. Dotted lines show the propagation of impulsive waves.

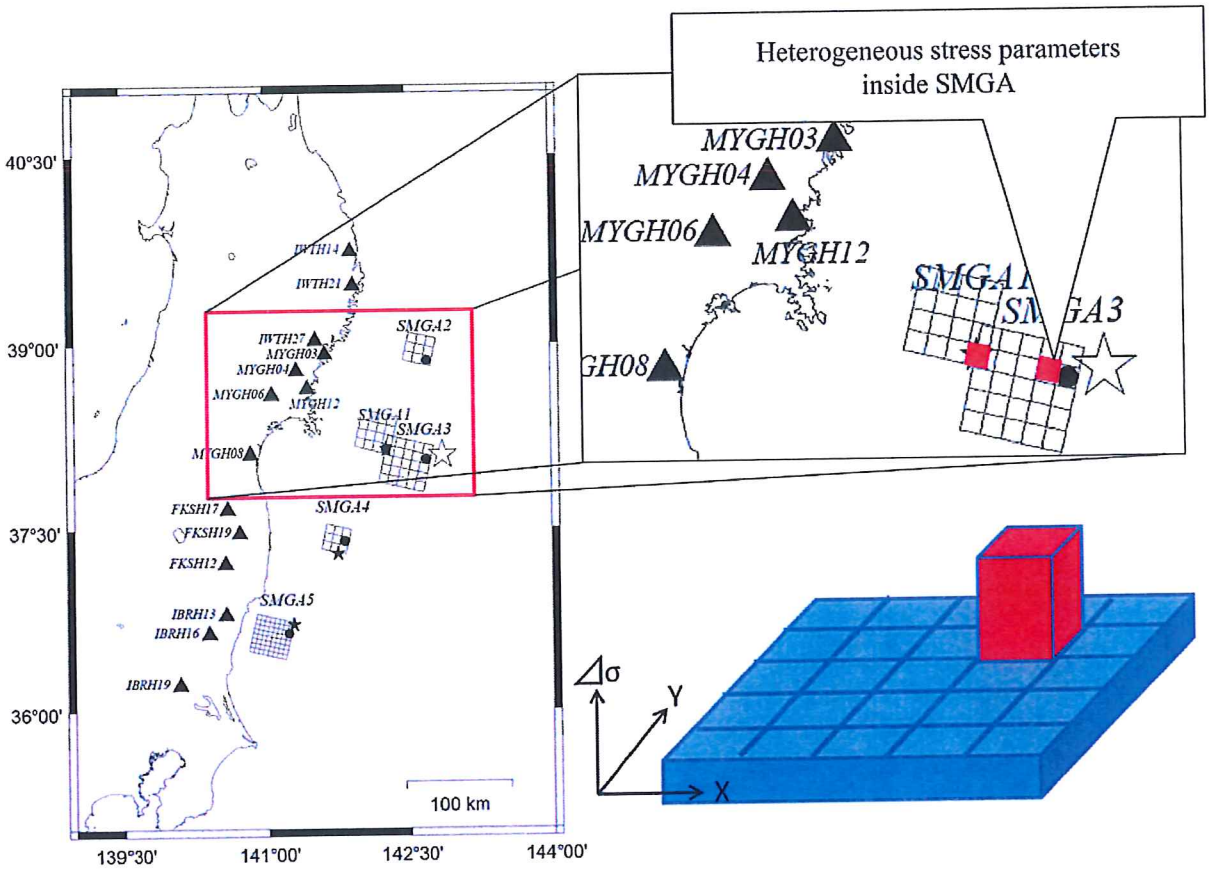

Figure 17. (Left) The short-period source model used in this study. (Upper right) Close-up illustration of strong-motion generation area 1 (SMGA1) and strong-motion generation area 3 (SMGA3). A higher stress parameter is included within the red cell. (Lower right) Heterogeneous SMGA model incorporating spatially varying stress parameters.

Comparison of Source Models from Short-Period and Long-Period Data

The 2011 Tohoku earthquake was observed by dense networks of geophysical instruments including teleseismic, strong-motion, tsunami, and geodetic instruments. Source models have been constructed using separate and joint inversions of various datasets and by forward modeling.

The short-period energy source region can also be constrained by the back-projection method (e.g., Ishii *et al.*, 2005) using regional network observations of teleseismic *P* waves, such as the North American, EU, and Tokyo Metropolitan arrays (e.g., Honda *et al.*, 2011; Ishii 2011; Koper *et al.*, 2011). Figure 20 shows energy release areas derived by Ishii (2011) from the back projection of short-period data for the 0.8–2.0 Hz frequency, compared with the locations of the SMGAs found in the present study.

The short-period source region described by Ishii (2011) is compact for an earthquake of this size and exhibits highly variable amounts of energy release in different portions. The predominant rupture propagation direction is along the strike in the southwestern direction, giving rise to the elongated rupture geometry of the earthquake overall. Subsidiary source regions extend to areas of rupture farther north and south than the regions that have been identified by other back-projection studies.

To first order, the short-period energy release areas obtained by Ishii (2011) are consistent with the locations of the SMGAs identified in our study. In detail, however, they differ slightly. According to Ishii (2011), the cyan contour in Figure 20 denotes the area that ruptured during subevent 1, within the first 40 s of the rupture, in an area west of the epicenter. The areas associated with the main phase and later bilateral rupture of subevent 2 are located west of sub event 1. Judging from the positions of the sources relative to the epicenter, subevent 1 occurred close to the hypocenter and then subevent 2 occurred later, west of subevent 1. Conversely, in our study, SMGA1 is inferred to have ruptured at almost the same time as subevent 1 of Ishii (2011) and SMGA3 to have ruptured later, east of SMGA1. We suggest that near-source strong-motion data provide more detailed information about the source geometry relative to the hypocenter than teleseismic back projection in this instance.

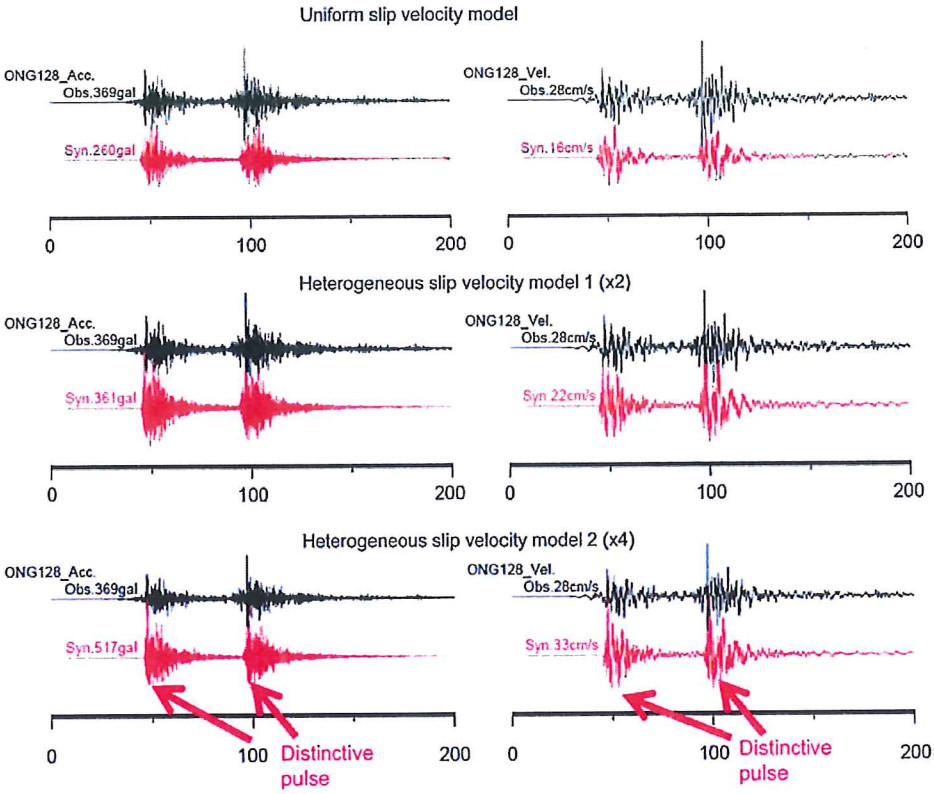

Figure 18. Comparison of observed and synthetic seismograms (north–south component) computed using a uniform model (top), a heterogeneous model with stress parameters increased by a factor of 4 (middle), and a heterogeneous model with stress parameters increased by a factor of 4 (bottom).

Figure 21 illustrates the slip distribution obtained by Yokota *et al.* (2011) from strong-motion data for the 10–100 s period band, once again compared with the locations of the SMGAs we have identified. The main rupture determined by Yokota *et al.* (2011) propagated in both the strike and dip directions, and extended into the deep area known as the Miyagi-Oki region and the compact shallow area near the Japan Trench. The estimate of Yokota *et al.* (2011) of the location of predominant slip west of the hypocenter agrees well with the locations of SMGA1 and SMGA3 found here.

The coseismic slip areas estimated using GPS data extend for ~100 km eastward of the hypocenter and for 150 km along the Japan Trench (Fig. 22a; Geospatial Information Authority of Japan, 2011; see Data and Resources). Tsunami data indicate that the source of the largest tsunami was located near the axis of the Japan Trench (Fujii *et al.*, 2011). Large amounts of slip on the plate interface in the southern Sanriku-oki (~30 m) and Miyagi-Oki (~17 m) areas surrounding the epicenter have been estimated from tsunami data (Fig. 22b).

The short-period energy source region constrained by back projection using regional network observations of teleseismic *P* waves is located along the down-dip portion of the megathrust, whereas the long-period source region is located near the axis of the Japan Trench. These results clearly reveal the frequency-dependent rupture process of the Tohoku earthquake, as described by Koper *et al.* (2011).

Discussion

The short-period source model we have described here reveals the involvement of at least five distinct SMGAs in the rupture process. In comparison, a long-term earthquake forecast for the region off the coast of Tohoku from Middle Sanriku-Oki to Ibaragi-Oki based on an ~400-year earthquake record has been made by the Japan Earthquake Research Committee (ERC), dividing the region into the six segments shown in Figure 23a. In undertaking the national seismic-hazard assessment, the ERC assumed that a characteristic earthquake of M 7–8 would occur with specified probability in each segment (ERC, 2009). The ERC did not anticipate a M_w 9 earthquake involving the simultaneous rupture of all of the fault segments. However, the segmentation identified in the hazard-assessment process based on previous earthquake activity does seem informative in terms of the short-period source model revealed by our analysis.

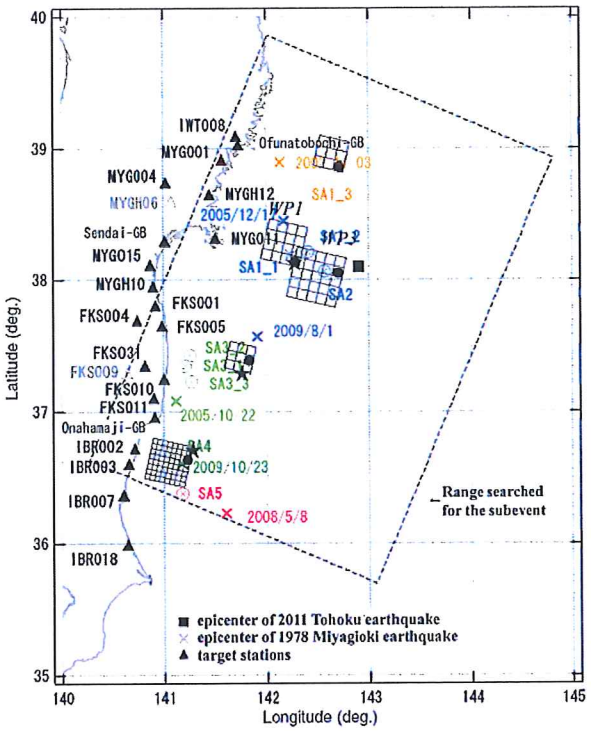

Figure 19. Comparison of the short-period source model obtained in this study and the super-asperity model of Nozu (2012).

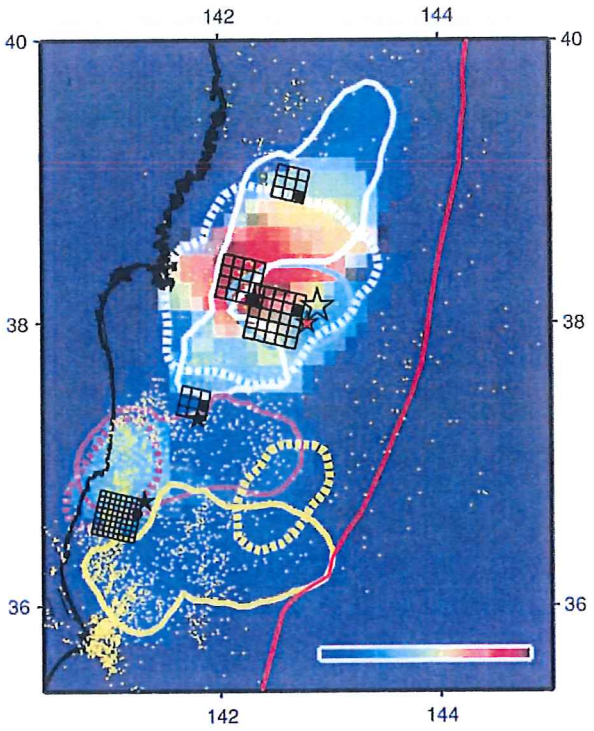

Figure 20. Comparison of the short-period source model obtained in this study with the high-frequency back-projection results of Ishii (2011). Warmer colors indicate greater high-frequency energy release. The cyan contour shows the area that first ruptured during subevent 1, and the two white lines delineate the areas that ruptured subsequently ruptured in subevent 2.

The five SMGAs are plotted on the ERC hazard map in Figure 23a. One SMGA is located in each segment except for the near-trench zone, which has mostly generated tsunami earthquakes and large tsunami in historic times but only relatively small short-period motions.

The slip distributions of previous medium-sized earthquakes of M 7 class (with a maximum M 7.5) are also plotted on the segments used for the long-term forecast in Figure 23b, although the slip inversion results are only available for recent earthquakes. One of the oldest earthquakes referred to here is the 1936 (M_w 7.4) Miyagi-ken-Oki event. The segments for the long-term forecast are consistent with the slip distributions of previous medium-sized earthquakes with $M < 8.05$. The sizes of the five SMGAs roughly correspond to those events.

Based on the results of our analysis, we have attempted to construct a recipe for predicting strong ground motions, to be applicable to future megathrust earthquakes. Irikura and Miyake (2010) developed such a recipe for predicting strong ground motions for inland earthquakes. They assumed that the large slip areas determined via waveform inversions using strong ground motion data coincide with the SMGAs, including short-period motions. We find in this study, however, that this assumption is invalid for megathrust earthquakes.

Nevertheless, a recipe for estimating the segments as inner-fault parameters is useful even for megathrust earthquakes. The segments of the source area can be deduced from the seismicity and geomorphological characteristics of the target region for megathrust as well as for inland earthquakes, and one or two SMGAs assigned to each segment. The average stress parameter for each SMGA should be assigned from empirical relations and has been found to be ~25 MPa in this study. The heterogeneity of stress parameters inside an SMGA should be considered within a specific range, which our results suggest equates to a factor of four.

Conclusions

We have constructed a short-period source model for the 2011 Tohoku earthquake using forward modeling by comparing the observed records with synthesized motions based on the characterized source model (Miyake *et al.*, 1999) and the EGR method (Irikura, 1986). The observed strong-motion records exhibit five distinct wavepackets that correspond to specific SMGA.

In the first part of the analysis, we attempted to identify the origins of the wavepackets using semblance analysis in order to determine the short-period source model more accurately. The origins of WP1, WP3, and WP5 are

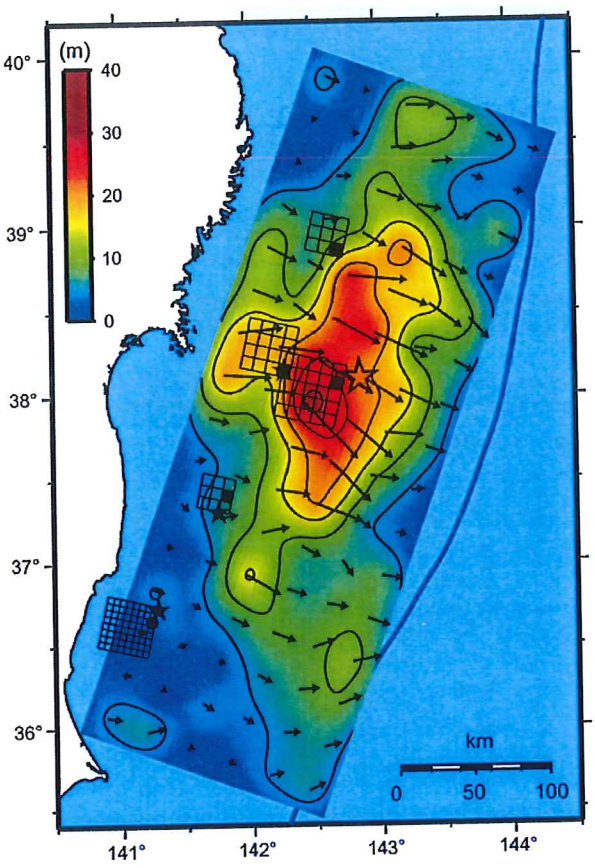

Figure 21. Comparison between the short-period source model obtained in this study and the slip distributions obtained by Yokota *et al.* (2011) via waveform inversion using band-pass-filtered (10–100 s) strong-motion data.

straightforwardly calculated because these three wavepackets are isolated from each other in the observed seismograms. The semblance values are projected onto an assumed source area on the mainshock fault plane using seismic-ray tracing and assuming uniform velocity structures. The origins of WP2 and WP4 have been estimated using the back-propagation method (Kurahashi and Irikura, 2010) because the waveforms of WP2 and WP4 are not temporally isolated in the observed seismograms.

Next, we successfully simulated ground motions from the five SMGAs using seismograms from nearby events as EGFs. SMGA1 is located in the source region of Miyagi-Oki, west of the hypocenter; SMGA2 in that of the middle Sanriku-Oki, north of the hypocenter; and SMGA3 in southern Sanriku-Oki, west of the hypocenter. Miyagi-oki is west of southern Sanriku-Oki. SMGA4 and SMGA5 are located near the down-dip edge of the mainshock source fault, ranging from offshore Fukushima prefecture to offshore Ibaraki prefecture. The 2005 M_w 7.2 Miyagi-Oki earthquake occurred near the origins of WP1 and WP3, and records of that earthquake likewise exhibit two wavepackets. We used the second of those wavepackets to construct EGFs containing the main *S*-wave motions and the *S*-wave coda for SMGA1 and SMGA3, and also for SMGA2 in the absence of a suitable nearby alternative. Observations of M 6 earthquakes occurring near the origins of WP4 and WP5 were used as EGFs for analyzing SMGA4 and SMGA5.

The locations of SMGA1 and SMGA3 roughly coincide with those identified by Asano and Iwata (2011; see Data and Resources) and by Satoh (2012).

At some stations near the source fault, impulsive waves within WP1 and WP3 are evident in the recorded seismograms. Ground motions with impulsive waves cannot be simulated using a uniform SMGA model. We have attempted to simulate the observed ground motions at ONG128 on the assumption that the SMGAs corresponding to WP1 and WP3 have heterogeneous stress parameters. The impulsive waves of WP1 and WP3 are well simulated using the heterogeneous model with higher stress parameters (by factors of 2 and 4, respectively) in the subarea of the corresponding SMGA. To specify the size of the heterogeneity more precisely, we will need to simulate ground motions using the records of smaller events as EGFs.

We have compared the short-period source model with rupture models obtained from other datasets. The short-period energy release from the back-projection of short-period data in the 0.8–2.0 Hz frequency range by Ishii (2011) extends westward from the hypocenter. Similarly, the areas of predominant slip identified by Yokota *et al.* (2011) from strong-motion records in the period range of 10–100 s also lie west of the hypocenter. Conversely, the coseismic slip area identified by GPS data extends eastward for a distance of ~100 km from the hypocenter and 150 km along the Japan Trench. The area of large slip inferred from tsunami data is located near the axis of the Japan Trench.

The SMGAs delineated in the present study are located along the down-dip portion of the megathrust. They thus coincide with the short-period energy source region obtained by Ishii (2011) and the areas of predominant slip by Yokota *et al.* (2011). Conversely, the short-period model differs appreciably from the long-period source model obtained using GPS and tsunami datasets.

In our short-period source model, one SMGA is located in each fault segment except for the near-trench zone. This suggests a recipe for predicting the strong ground motions produced by future megathrust earthquakes by assigned SMGAs to fault segments of interest.

Data and Resources

The strong-motion records obtained by the National Research Institute for Earthquake Science and Disaster Prevention (NIED) and used in this article can be retrieved from K-NET and KiK-net (www.kyoshin.bosai.go.jp/kyoshin/; last accessed September 2012). The strong-motion seismograms used in this study were provided by the Tohoku

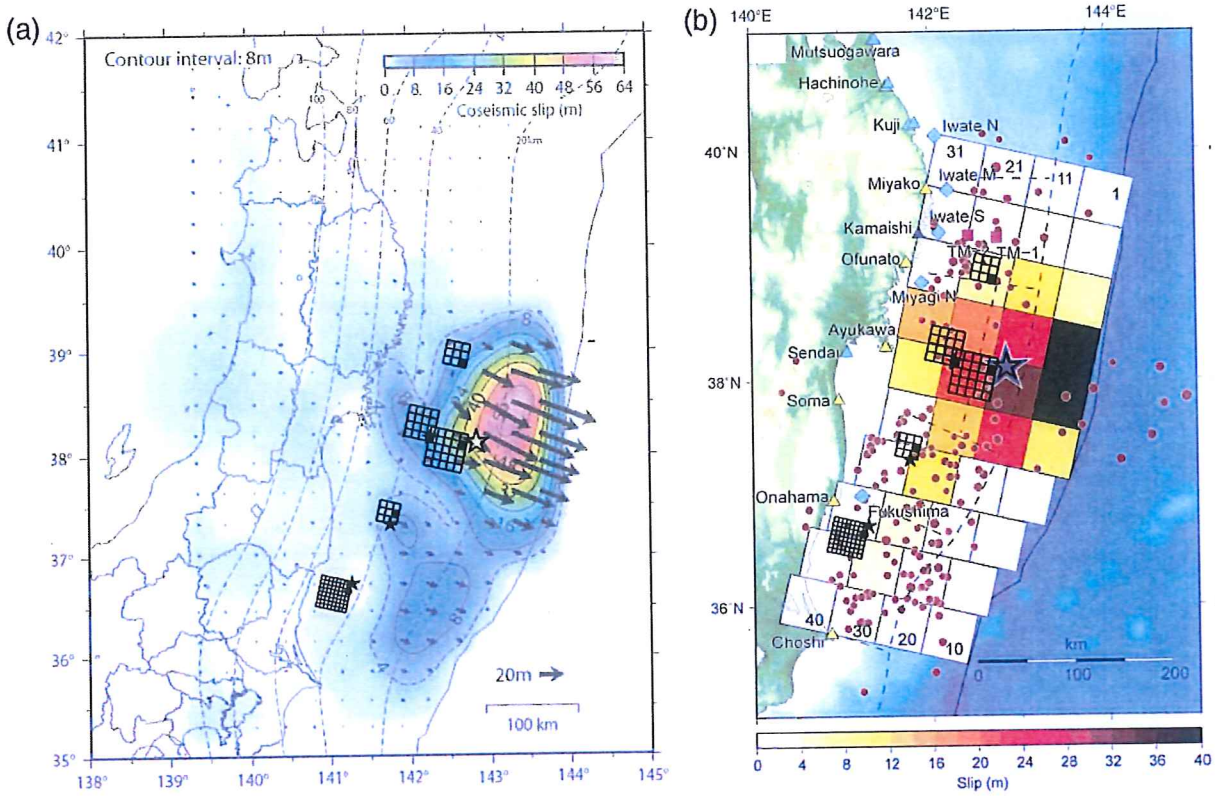

Figure 22. The short-period source model obtained in this study plotted on top of (a) the slip distribution computed from inland and offshore Global Positioning System (GPS) data (Geospatial Information Authority of Japan, 2011; see Data and Resources) and (b) the slip distribution inferred from tsunami data (Fujii *et al.*, 2011).

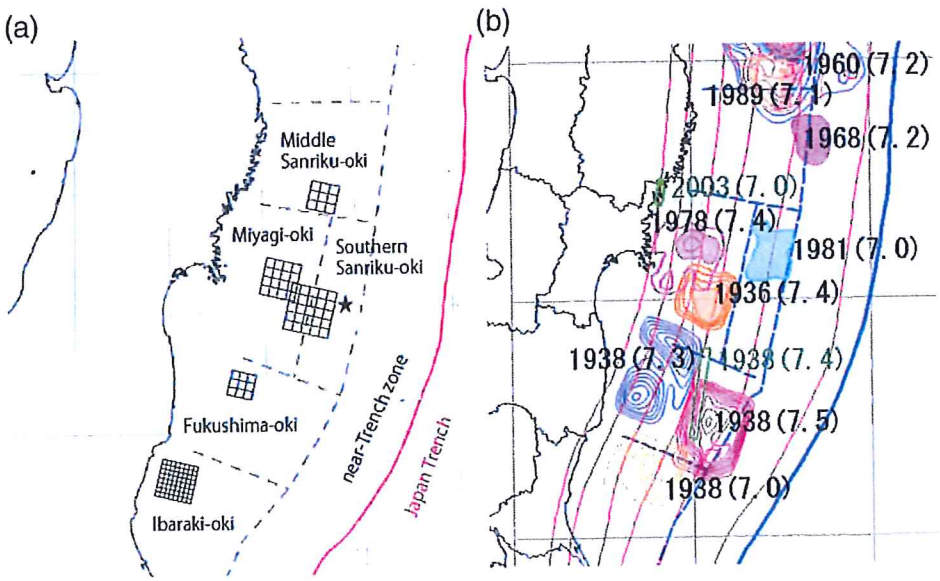

Figure 23. (a) The short-period source model and source segments used for the long-period forecast by the Japan Earthquake Research Committee (ERC). (b) Source segments for the long-period forecast and the slip distributions of past earthquakes (Earthquake Research Committee [ERC], 2009).

Electric Power Corporation, Japan. Data are available from the Japan Association for Earthquake Engineering site (www.jaee.gr.jp/jp/stack/data/; last accessed September 2012). Moment-tensor solutions can be obtained from the F-net web site (www.fnet.bosai.go.jp/top.php; last accessed September 2012). Details on fatalities and missing persons are provided by the Fire and Disaster Management Agency and are available on its website (www.fdma.go.jp/bn/higaihou/pdf/jishin/144.pdf; last accessed September 2012). Asano and Iwata's (2011) source model is available at http://sms.dpri.kyoto-u.ac.jp/k-asano/pdf/ssj2011_a11-06.pdf (last accessed September 2012). The slip distribution on the plate interface computed by the Geospatial Information Authority of Japan is available at www.gsi.go.jp/cais/topic110520-index.htm (last accessed September 2012). Kamae and Kawabe's (2011) source model is available at www.rri.kyoto-u.ac.jp/jishin/eq/tohoku3/SourceParaRev20110617.pdf (last accessed September 2012) and Yamanaka's (2011) model is available at www.seis.nagoya-u.ac.jp/sanchu/Seismo_Note/2011/NGY36n.html (last accessed September 2012). We used the Generic Mapping Tools of Wessel and Smith (1995) to draw the figures.

Acknowledgments

We are deeply appreciative of comments provided by the Associate Editor and reviewers. We would like to express our gratitude to the National Research Institute for Earth Science and Disaster Prevention (NIED) and the Tohoku Electric Power Corporation, Japan, for providing the strong-motion data supporting this study.

References

Brune, J. N. (1970). Tectonic stress and the spectra of seismic shear waves from earthquakes, *J. Geophys. Res.* **75,** 4997–5009.

Brune, J. N. (1971). Correction, *J. Geophys. Res.* **76,** 5002.

Earthquake Research Committee (ERC) (2009). Long-term forecast of earthquakes from Sanriku-Oki to Boso-Oki (revised; in Japanese), 80 pp., Headquarters for Earthquake Research Promotion.

Fujii, Y., K. Satake, S. Sakai, M. Shinohara, and T. Kanazawa (2011). Tsunami source of the 2011 Off the Pacific Coast of Tohoku earthquake, *Earth Planets Space* **63,** 815–820.

Honda, R., S. Aoi, H. Sekiguchi, and H. Fujiwara (2008). Imaging an asperity of the 2003 Tokachi-Oki earthquake using a dense strong-motion seismograph network, *Geophys. J. Int.* **172,** 1104–1116.

Honda, R., Y. Yukutake, H. Ito, M. Harada, T. Aketagawa, A. Yoshida, S. Sakai, S. Nakagawa, N. Hirata, K. Obara, and H. Kimura (2011). A complex rupture image of the 2011 Off the Pacific Coast of Tohoku earthquake revealed by the MeSO-net, *Earth Planets Space* **63,** no. 7, 583–588.

Ide, S., A. Baltay, and G. Beroza (2011). Shallow dynamic overshoot and energetic deep rupture in the 2011 M_w 9.0 Tohoku-Oki earthquake, *Science* **336,** no. 6036, 1426–1429, doi: 10.1126/science.1207020.

Irikura, K. (1986). Prediction of strong acceleration motions using empirical Green's function, in Proc. 7th Japan Earthq. Eng. Symp., Tokyo, 10–12 December, 151–156.

Irikura, K., and K. Kamae (1994). Estimation of strong ground motion in broad-frequency band based on a seismic source scaling model and an empirical Green's function technique, *Ann. Geofisc.* **37,** no. 6, 1721–1743.

Irikura, K., and H. Miyake (2010). Recipe for predicting strong ground motion from crustal earthquake scenarios, *Pure Appl.Geophys.* **168,** nos. 1–2, 85–104.

Irikura, K., T. Kagawa, and H. Sekiguchi (1997). Revision of the empirical Green's function method by Irikura (1986), Program and abstracts, *Seismol. Soc. Japan* **2,** B25 (in Japanese).

Ishii, M. (2011). High-frequency rupture properties of the M_w 9.0 Off the Pacific Coast of Tohoku earthquake, *Earth Planets Space* **63,** no. 7, 609–614.

Ishii, M., P. M. Shearer, H. Houston, and J. E. Vidale (2005). Extent, duration and speed of the 2004 Sumatra–Andaman earthquake imaged by the Hi-net array, *Nature* **435,** 933–936.

Kamae, K., and K. Irikura (1998). Rupture process of the 1995 Hyogo-ken Nanbu earthquake and simulation of near-source ground motion, *Bull. Seismol. Soc. Am.* **88,** 400–412.

Kataoka, S., T. Kusakabe, J. Murakoshi, and K. Tamura (2003). Study on a procedure for formulating level 2 earthquake motion-based on scenario earthquakes, Research Report of National Institute for Land and Infrastructure Management, Vol. 15.

Kawase, H., and H. Matsuo (2004). Relationship of *S*-wave velocity structures and site effects separated from the observed strong-motion data of K-NET, KiK-net, and JMA network, *J. Japan Assoc. Earthq. Eng.* **4,** no. 1, 33–52.

Koketsu, K., Y. Yokota, N. Nishimura, Y. Yagi, S. Miyazaki, K. Satake, Y. Fujii, H. Miyake, S. Sakai, Y. Yamanaka, and T. Okada (2011). A unified source model for the 2011 Tohoku earthquake, *Earth Planet. Sci. Lett.* **310,** nos. 3–4, 480–487, doi: 10.1016/j.epsl.2011.09.009.

Koper, K. D., A. R. Hutko, T. Lay, C. J. Ammon, and H. Kanamori (2011). Frequency-dependent rupture process of the 2011 M_w 9.0 Tohoku earthquake: Comparison of short-period *P*-wave back-projection images and broadband seismic-rupture models, *Earth Planets Space* **63,** no. 7, 599–602.

Kurahashi, S., and K. Irikura (2010). Characterized source model for simulating strong ground motions during the 2008 Wenchuan earthquake, *Bull. Seismol. Soc. Am.* **100,** 2450–2475.

Kurahashi, S., and K. Irikura (2011). Source model for generating strong ground motions during the 2011 Off the Pacific Coast of Tohoku earthquake, *Earth Planets Space* **63,** no. 7, 571–576.

Kurahashi, S., K. Masaki, and K. Irikura (2008). Source model of the 2007 Noto-Hanto earthquake (M_w 6.7) for estimating broadband strong ground motion, *Earth Planets Space* **60,** no. 2, 89–94.

Matsushima, S., and H. Kawase (2006). Proposal of super-asperity model for subduction earthquakes (in Japanese), *Monthly Chikyu* **55,** no. 55, 98–102.

Miyake, H., T. Iwata, and K. Irikura (1999). Strong ground motion simulation and source modeling of the Kagoshima-ken Hokuseibu earthquake of March 26 (M_{JMA} 6.5) and May 13 (M_{JMA} 6.3), 1997, using empirical Green's function method, *Zisin* **51,** 431–442 (in Japanese with English abstract).

Nozu, A. (2012). A super asperity model for the 2011 Off the Pacific Coast of Tohoku earthquake, *J. Japan Assoc. Earthq. Eng.* **12,** no. 2, 21–40 (in Japanese with English abstract).

Nozu, A., and T. Sugano (2006). Simulation of strong ground motions from shallow crustal and subduction-zone earthquakes based on site-specific amplification and phase characteristics, Technical note of the Port and Airport Research Institute No. 1120, 1–34 (in Japanese with English abstract).

Nozu, A., T. Nagao, and M. Yamada (2009). Simulation of strong ground motions using empirical site amplification and phase characteristics: Modification to incorporate causality (in Japanese with English abstract), *J. Japan Soc. Civil Eng.* **65,** 808–813.

Ozawa, S., T. Nishimura, H. Suito, T. Kobayashi, M. Tobita, and T. Imakiire (2011). Coseismic and post-seismic slip of the 2011 M_w 9.0 Tohoku-Oki earthquake, *Nature* **475,** 373–376.

Satoh, T. (2012). Source modeling of the 2011 Off the Pacific Coast of Tohoku earthquake using empirical Green's function method: From

the viewpoint of the short-period spectral level of interplate earthquakes, *J. Struct. Constr. Eng., AIJ* no. 675, 695–704.

Spudich, P., and D. Oppenheimer (1986). Dense seismograph array observations of earthquake rupture dynamics, in *Earthquake Source Mechanics*, S. Das, J. Boatwright, and C. H. Scholz (Editors), Maurice Ewing Series 6, AGU, Washington, 285–296.

Suzuki, W., and T. Iwata (2007). Source model of the 2005 Miyagi-Oki, Japan, earthquake estimated from broadband strong motions, *Earth Planets Space* **59,** 1155–1171.

Yagi, Y., and Y. Fukahata (2011). Rupture process of the 2011 Tohoku-Oki earthquake and absolute elastic strain release, *Geophys. Res. Lett.* **38,** no. 19, L19307, doi: 10.1029/2011GL048701.

Yokota, Y., K. Koketsu, Y. Fujii, K. Satake, S. Sakai, M. Shinohara, and T. Kanazawa (2011). Joint inversion of strong motion, teleseismic, geodetic, and tsunami datasets for the rupture process of the 2011 Tohoku earthquake, *Geophys. Res. Lett.* **38,** L00G21, doi: 10.1029/2011GL050098.

Wessel, P., and W. Smith (1995). New version of the generic mapping tools, *Eos Trans. AGU* **76,** 329.

Aichi Institute of Technology
1247 Yachigusa, Yakusa-cho
Toyota-shi, Aichi 470-0392, Japan
susumu@aitech.ac.jp
(S.K.)

Disaster Prevention Research Center
Aichi Institute of Technology
1247 Yachigusa, Yakusa-cho
Toyota-shi, Aichi 470-0392, Japan
irikura@geor.or.jp
(K.I.)

Manuscript received 26 April 2012